Materials Science & Engineering A 620 (2014) 16–21

Contents lists available at ScienceDirect

Materials Science & Engineering A

journal homepage: www.elsevier.com/locate/msea

A physical model revealing strong strain hardening in nano-grained metals induced by grain size gradient structure

Jianjun Li [a,*], Shaohua Chen [b], Xiaolei Wu [b], A.K. Soh [c]

[a] Department of Engineering Mechanics, School of Mechanics, Civil Engineering and Architecture, Northwestern Polytechnical University, Xi'an 710129, Shanxi, People's Republic of China
[b] State Key Laboratory of Nonlinear Mechanics, Institute of Mechanics, Chinese Academy of Sciences, Beijing 100190, People's Republic of China
[c] School of Engineering, Monash University Malaysia, Bandar Sunway, Salangor, Malaysia

ARTICLE INFO

Article history:
Received 11 August 2014
Received in revised form
29 September 2014
Accepted 30 September 2014
Available online 7 October 2014

Keywords:
Grain size gradient structure
Extra strain hardening
Ductility
Geometrically necessary dislocations
Nano-grained metal

ABSTRACT

A theoretical model has been developed, which reveals the underlying correlation between the strong extra strain hardening achieved in the nano-grained layers of the grain size gradient structure and the non-uniform deformation of the lateral surface in surface nano-crystallized materials, based on some existing experimental observations and the concept of geometrically necessary dislocations. The proposed model led to the establishment of a simple physical law that can be expressed as $H^* = A^*$, where H^* and A^* are two dimensionless parameters. The former represents the extra strain hardening, while the latter characterizes the non-uniform deformation of the lateral surface. The values of these two parameters can be measured through experiments.

1. Introduction

Nano-grained metals and alloys are usually strong but brittle. Generally, their ultra-high strength and hardness (up to several gigapascals) are achieved at the expense of their ductility, which is typically less than a few percent in terms of uniform elongation, due to the suppression of the conventional dislocation slip that dominates in their coarse-grained (CG) counterparts [1–3]. The brittleness of nano-grained metals/alloys is a severe setback to their practical applications. In the past decades, various strategies have been proposed to enhance the ductility of nano-grained materials while maintaining their superior strength, which include growth stimulating of nano-grains by stress [4–8], evoking of abundant dislocation activities in nano-grains [9], embedding of high density coherent nanoscale twin boundaries in submicrometer-sized grains (called nano-twinned metals) [10,11], inserting of submicrometer-sized grains into nanocrystalline matrix (called bimodal metals) [12], sandwiching of a CG core by two grain size gradient (GSG) surface layers (called surface nano-crystallized (SNC) materials) [13,25,27,29], etc. Note that the grain size in the GSG layer of SNC materials varies along the thickness dimension from tens of nanometers in the topmost surface to tens of micrometers at the core.

SNC materials have attracted intensive scientific interests due to their cost effectiveness and amenability to large scale production methodology, i.e., surface severe plastic deformation (S^2PD) [13,14]. S^2PD have many variants, such as shot peening[15], air blast shot peening [16], sandblasting [17], cryogenic burnishing [18], particle impact processing [19], surface nano-crystallization and hardening [20], ultrasonic shot peening [21], surface mechanical attrition treatment (SMAT) [13] and surface mechanical grinding treatment (SMGT) [14]. The unique GSG structure usually renders outstanding balance of high strength and ductility in nanostructured materials. For example, a SNC copper sample fabricated by SMGT possesses a uniform tensile elongation comparable to that of a CG copper sample, and the strength of the former is double that of its CG counterpart [14]. Another example is a SNC Ni sample with a Ni–P amorphous coating in which the amorphous layer gained a 12% uniform tensile elongation [22]. Such high magnitude of tensile ductility is exceptional in metallic amorphous materials.

In the past decades, most of the works carried out on SNC materials were mainly focused on the following aspects: (1) grain refinement mechanism in the GSG structure [23]; (2) mechanical behavior of materials [24]; (3) major factors that affected mechanical properties [20,25]; (4) optimization parameters for achieving favorable properties based on surface nanocrystallization techniques

* Corresponding author.
E-mail addresses: jianjunli.mech@gmail.com, mejjli@nwpu.edu.cn (J. Li).

http://dx.doi.org/10.1016/j.msea.2014.09.117
0921-5093/

[26,27]; (5) characterization of the plastic properties in the GSG layer [28]; and (6) development of quantitative continuum plasticity models for SNC materials [29].

In spite of the above progress, the specific mechanism that leads to a good balance of strength and ductility in SNC materials is still not well understood. Most recently, Wu et al. [30] reported successful fabrication of SNC interstitial free (IF) steel samples that possessed a tensile ductility comparable to the corresponding CG samples, and the yield strength of the former was 1.6 times higher than that of their CG counterparts. Moreover, they observed a strong strain hardening behavior, which was an additional gain in the nano-grained layers of the GSG region in the SNC IF steel sample. They attributed the extra strain hardening to the non-uniform deformation in the lateral surface. However, the critical issue of how the non-uniform lateral surface deformation induces the extra hardening has yet to be addressed. Therefore, in the present study a physical model will be developed to quantitatively correlate the non-uniform deformation in the lateral surface of the SNC sample with the extra strain hardening achieved in the GSG layer based on the experimental observations made by Wu et al. [30] and the concept of geometrically necessary dislocations (GNDs) [31–34].

2. Experimental review

Fig. 1 presents the variation of microhardness increment ΔH with respect to sample depth h, which was reported by Wu et al. [30] after testing the SNC IF steel samples fabricated by SMAT to various uniaxial tensile strains. The parameter ΔH is defined as the difference between the hardness along the thickness dimension of a SNC sample '*after*' and '*before*' a tensile test. This parameter is an indicator for the level of strain hardening retained after unloading. A strong extra strain hardening ΔH_g was observed along the thickness dimension of the sample, as indicated by the vertical short dashed lines in Fig. 1 for tensile engineering strain $\varepsilon_e = 0.25$. The value of ΔH for a free standing GSG layer of 120 μm thickness at failure, i.e., $\varepsilon_e = 0.05$, is also included as a reference to calculate ΔH_g. The maximum value of ΔH_g in the GSG layer of a SNC sample could reach as high as 527.5 MPa at $h = 93.6$ μm for $\varepsilon_e = 0.25$. They concluded that the remarkable extra stain hardening in the GSG structure led to the extraordinary synergy of strength and ductility in the SNC IF steel sample.

Moreover, it can be seen from Fig. 1 that the trends of the hardness increment ΔH versus the sample depth h for different strains ($\varepsilon_e = 0.05, 0.1, 0.25$) are identical, i.e., ΔH first increases to a maximum and then decreases till the appearance of a plateau, which represents the hardness increment of the CG core. The ΔH peak gradually moves toward the CG core as the strain increases; and it eventually enters the CG core and reaches $h \approx 180$ μm as the strain is increased up to 0.25.

These findings indicate that the extra hardening ΔH_g occurs not only in the GSG layer but also in the CG core for all cases of the applied strain. The ΔH_g in the CG core is given by the height difference between the curve and the horizontal dashed line in the CG region, as shown in Fig. 1. The appearance of ΔH_g in both the GSG and CG regions has been attributed to the non-uniform deformation in the lateral surface induced by the mutual constraint between the GSG surface layers and the CG core during the uniaxial tensioning (Fig. 3 in [30]). In this study, a physical model will be developed to establish a quantitative correlation between ΔH_g and the lateral non-uniform deformation based on the concepts of GNDs. Indeed, the range of ΔH_g tallies exactly to that of the lateral non-uniform deformation in a SNC sample. For example, the range of ΔH_g is $h \in [0, 340\ \mu m]$ for an applied strain of 0.25 (Fig. 1), which is approximately identical to that of the lateral non-uniform deformation (Fig. 5).

3. Model description

In the present study, for clear illustration the SNC sample is simply modeled as a perfectly bonded multi-layered structure with various layers of different grain sizes as shown in Fig. 2(a). The grain size in the same layer is assumed to be homogeneous according to the experimental observation [30]. The proposed model consists of two GSG surface layers sandwiching a CG core. The blue dashed lines indicate the boundaries between the hypothesized layers. The areas in orange represent two GSG regions in the model. Fig. 2(b) presents a schematic diagram of the non-uniform deformation in the lateral surface (vertical to the x-axis) by maintaining the uniaxial tension at a given strain before the occurrence of necking, as observed in experiments [30]. The non-uniform deformation is characterized by a parameter u, which is defined as the height profile of the lateral surface after deformation. The rationale for the non-uniform deformation could be explained by a special stress state in the SNC sample as follows.

Generally, the freestanding layers with smaller grain size are prone to plastic instability (or necking in the lateral direction, i.e., x-axis in Fig. 2a) at smaller tensile strain as compared with those of larger grain size. However, in the case of SNC sample with a grain size gradient structure, the faster lateral necking of those layers with smaller grain size (i.e., outer layers) is suppressed by the higher plasticity of layers with larger grain size (i.e., inner layers). As a result, the mutual constraints between various layers of different grain sizes lead to a three-dimensional stress state in

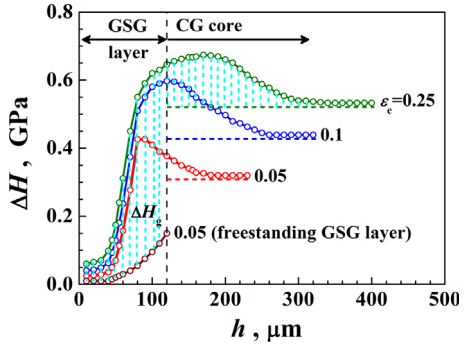

Fig. 1. Variation of hardness increment ΔH of SNC IF steel samples subjected to various tensile strains (i.e., $\varepsilon_e = 0.05$, 0.1 and 0.25) with respect to the depth h [25]. The vertical short dashed lines represent the extra hardening (i.e., ΔH_g) achieved in the GSG structure resulting from the non-uniform deformation in the lateral surface for $\varepsilon_e = 0.25$.

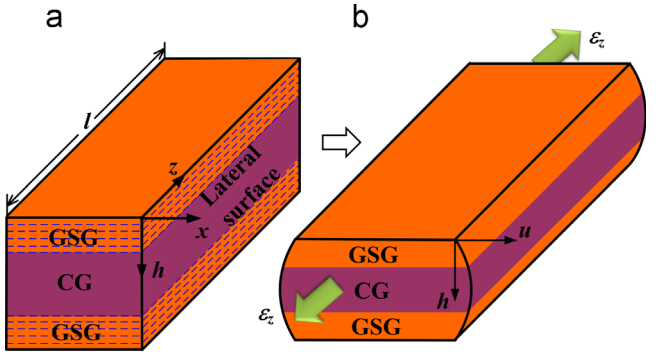

Fig. 2. Schematic diagram of a SNC sample subjected to a uniform tensile strain ε_z: (a) before tensioning and (b) after tensioning before the occurrence of necking. The SNC sample consists of two grain size gradient (GSG) surface layers sandwiching a coarse-grained (CG) core. (For interpretation of the references to color in this figure, the reader is referred to the web version of this article.)

the gradient structure of the SNC sample subjected to uniaxial tension.

To achieve a better understanding of the stress state in a SNC sample during uniaxial tensioning, a representative unit layer in the GSG structure is selected for analysis, as shown in Fig. 3(a). The stress states in all unit layers are identical except the outermost layers with a free surface. Due to the fact that the capacity to resist lateral instability is different from one layer to another, the shear stresses in the upper surface of the unit layer considered point toward the symmetrical plane (indicated by the dashed line) and those in the lower surface point outward (Fig. 3a). Moreover, the shear stress is non-uniformly distributed along the x-direction. The shear stress should be zero at the symmetrical plane as well as at the lateral surface, and it approaches a maximum at some location between the symmetrical plane and the lateral surface according to the results of some shear-lag and finite element analysis for multilayered structures [35,36]. The values of the shear stress along the assumed layer interfaces are denoted by the length of the arrows in Fig. 3(a). The above stress state ultimately leads to a non-uniform deformation in the lateral surface along the sample depth h, as schematically indicated by the curved boundary in Fig. 3(a). Thus, we may infer that the adoption of a gradient structure leads to the conversion of stress state from one dimension (uniaxial tension along z direction) in a homogeneous sample to three dimensions (simultaneous existence of tensions in z and x directions and pure shear in the xy plane) in a SNC sample, as shown in Fig. 3(b).

It has been widely accepted by researchers that nonuniform deformation is usually accommodated by GNDs [31–33]. In this section, we will develop a physical model to correlate the non-uniform deformation in the lateral surface (Fig. 3 in [30]) with the extra strain hardening (ΔH_g in Fig. 1) achieved in the GSG layer of the SNC sample based on the concept of GNDs. Fig. 4(a) presents a schematic diagram of the GNDs induced by the non-uniform deformation near the lateral surface of the GSG layer. A unit layer of thickness Δh is selected for analysis. The value of Δh is assumed

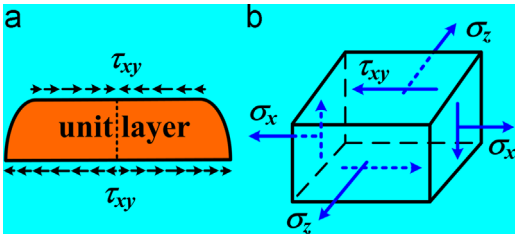

Fig. 3. Stress state of a SNC sample during uniaxial tensile deformation: (a) shear stress state in a unit layer and (b) 3-D stress state in the gradient structure.

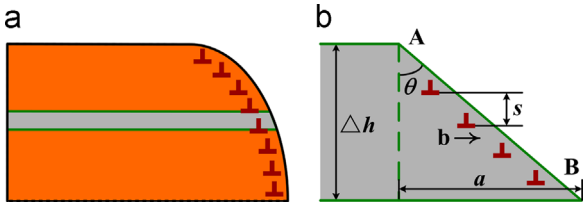

Fig. 4. The geometrically necessary dislocations (GNDs) in a SNC sample subjected to uniaxial tension. (a) GNDs near the deformed lateral surface in the GSG region; (b) GNDs in a unit layer (gray area in (a)), whose thickness Δh is assumed to be small enough such that the deformed lateral surface can be approximated as a straight plane, that is, 'AB' can be viewed as a straight line. The GNDs in (b) are assumed to be uniformly distributed in a cuboidal region adjacent to the deformed lateral surface in the unit layer with an equal spacing s; and the dislocation line of GNDs is idealized as a straight line running through the entire sample along the tensile direction.

to be small enough such that the deformed lateral surface can be approximated as a straight plane, that is, 'AB' can be viewed as a straight line. It is assumed that the GNDs are spaced equally along the sample depth h near the deformed lateral surface in the unit layer. Thus, we have

$$\tan\theta = \frac{a}{\Delta h} = \frac{b}{s} \tag{1}$$

where θ is the angle created by the non-uniform deformation between two adjacent unit layers, a is the height difference along the x-axis between two adjacent deformed unit layers, as shown in Fig. 4(b) ($a > 0$); b is the magnitude of Burger's vector of the GNDs, and s is the spacing between individual slip steps near the lateral surface, which is given by

$$s = \frac{b}{a}\Delta h \tag{2}$$

In the present analysis, the dislocation line of each GND is idealized as a straight line running through the entire sample along the tensile direction. Therefore, the total length of the injected GNDs due to the non-uniform lateral deformation, i.e., λ, in the unit layer with thickness Δh can be expressed as

$$\lambda = \frac{l\Delta h}{s} = \frac{la}{b} \tag{3}$$

where l is the total length of the tensile SNC sample, as shown in Fig. 2(a). To calculate the density of GNDs in the deformed SNC sample, we assume that all GNDs are uniformly distributed in a localized cuboidal region near the deformed lateral surface in a unit layer. The dimensions of the localized region are approximated as $\Delta h \times l \times \Delta h$, which leads to a volume V given by

$$V = l(\Delta h)^2 \tag{4}$$

Thus, the density of GNDs resulting from the non-uniform deformation that occurs in a grain size gradient structure is given by

$$\rho_{GSG} = \frac{\lambda}{V} = \frac{a}{b(\Delta h)^2} \tag{5}$$

By using Taylor's relation to correlate the shear strength τ with the total dislocation density ρ_T in a unit layer, we obtain

$$\tau = \alpha\mu b\sqrt{\rho_T} = \alpha\mu b\sqrt{\rho_s + \rho_{GB} + \rho_{GSG}} \tag{6}$$

where ρ_s, μ and α are the density of the statistically stored dislocations, the shear modulus of the material and an empirical constant that could be taken as 0.2–0.5, respectively; ρ_{GB} is the dislocation density arising from the strain gradient due to a sharply increased volume fraction of the GB region as grain size approaches nanoscale. The value of ρ_{GB} is proportional to $1/d$, where d is the grain size [37,38].

Von Mises flow rule is then employed to correlate the equivalent flow stress σ with the shear strength τ. The material in one layer can be viewed as homogeneous since the grain size in the same layer of a SNC sample is identical as observed in existing experiments [30]. Therefore, it is deemed reasonable to take Tabor's factor as 3 for the material in each layer for converting the equivalent flow stress σ to hardness H along the sample depth h after tensioning:

$$\sigma = \sqrt{3}\tau, \quad H = 3\sigma \tag{7}$$

in which the values of σ and H depend on the sample depth. By inserting Eqs. (5) and (6) into Eq. (7), we obtain

$$H = \sqrt{H_0^2 + \mu^2\frac{a}{a^*}} \tag{8}$$

where $H_0 = 3\sqrt{3}\alpha\mu b\sqrt{\rho_s + \rho_{GB}}$ is the hardness of a homogeneous sample after tensioning without non-uniform deformation; and

$a^* = (\Delta h)^2/(27\alpha^2 b)$ is a length parameter depending on the magnitude of Burger's vector of GNDs and the value of Δh. On the other hand, the extra hardening ΔH_g can be expressed as (see the vertical dashed lines in Fig. 1):

$$\Delta H_g = \Delta H_{SNC} - \Delta H_{free\ GSG} \tag{9}$$

where $\Delta H_{SNC} = H^a_{SNC} - H^b_{SNC}$ and $\Delta H_{free\ GSG} = H^a_{free\ GSG} - H^b_{free\ GSG}$ in which ΔH is the hardness enhancement during deformation (Fig. 1). The subscripts 'SNC' and 'free GSG' represent SNC sample and free standing GSG layer, respectively, while the superscripts '*a*' and '*b*' denote *after* and *before* tensile deformation, respectively. Note that an approximation has been adopted in Eq. (9) to calculate ΔH_g. The ΔH values of various free standing layers with different grain sizes have been replaced by those of the layers in a free standing GSG sample at $\varepsilon_e = 0.05$, i.e., $\Delta H_{free\ GSG}$, due to the impossibility of measuring the ΔH value of the free standing layers. The approximation would not produce significant errors in calculating ΔH_g since the thickness of GSG region is very small as compared with that of the whole SNC sample. By ignoring the effect of residual stresses on the hardness of SNC sample, i.e., $H^b_{SNC} = H^b_{free\ GSG}$, we obtain

$$\Delta H_g = H^a_{SNC} - H^a_{free\ GSG} = H - H_0 \tag{10}$$

By inserting the above expression into Eq. (8), we have

$$\frac{\Delta H_g(2H - \Delta H_g)}{\mu^2} = \frac{a}{a^*} \tag{11}$$

Note that the free standing GSG layer fails at 5% strain, thus the value of $\Delta H_{free\ GSG}$ approaches maximum at this strain, which can be used as a reference value to calculate ΔH_g for various strains. Specifically, in the present analysis, the value of ΔH_g can be calculated as follows using the case of $\varepsilon_e = 0.25$ as an example: $\Delta H_g(\varepsilon_e = 0.25,\ h) = \Delta H_{SNC}(\varepsilon_e = 0.25,\ h) - \Delta H_{free\ GSG}(\varepsilon_e = 0.05,\ h)$ (refer to the vertical short dashed lines in Fig. 1). The values of H, ΔH_g and a depend on the distance between the unit layer considered and the top surface, i.e., the sample depth h; these three values can be measured through experiments. The above equation can be written in a simple form as follows:

$$H^* = A^* \tag{12}$$

where $H^* = \Delta H_g(2H - \Delta H_g)/\mu^2$ and $A^* = a/a^*$ are two dimensionless parameters, which represent the extra strain hardening achieved in the GSG region and the non-uniform lateral surface deformation, respectively. In the following calculations, the shear modulus is set as a constant along the sample depth, as observed in the experiments for a SNC copper sample [39], i.e., $\mu = 77$ GPa for SNC IF steel. The value of α and b are set as 0.3 and 0.25 nm, respectively. The value of Δh can be determined by fitting the values of the two parameters.

4. Results and discussion

All the experimental data for height profiles in the range of $h \in (0, 50\ \mu m)$ were significantly influenced by noise and some were unavailable due to the roughness of the lateral surface and the limitation of the instrument. A Matlab function, i.e., fnval, was used to smoothen the eight measured height profiles in the range of $h \in (50, 300\ \mu m)$ in order to facilitate the derivation of the parameter a (see the short dashed lines for each profile in Fig. 5). The red solid line in Fig. 5 represents the arithmetic average of the eight smoothened height profiles for calculating the value of parameter a. As a result, parameter a becomes the product of the slope of u versus h and the thickness of one unit layer as shown in Fig. 5, i.e., $a = (du/dh)\Delta h$.

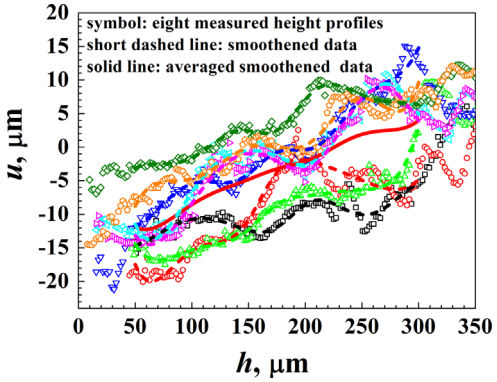

Fig. 5. Height profiles (u versus h) used in the present analysis. The eight height profiles were measured across the lateral surface (vertical to the x-axis, see Fig. 2) within the uniform deformation section after applying tensile strain of 0.25 [30]. The eight profiles were smoothened and averaged arithmetically to calculate the value of parameter a, see the red solid line. (For interpretation of the references to color in this figure legend, the reader is referred to the web version of this article.)

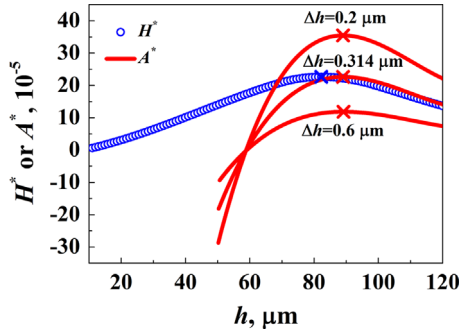

Fig. 6. Comparison of two sample depth-dependent dimensionless parameters, i.e., $H^* = \Delta H_g(2H - \Delta H_g)/\mu^2$ and $A^* = a/a^*$ for a SNC IF steel sample at $\varepsilon_e = 0.25$ for three cases of Δh, i.e., $\Delta h = 0.2,\ 0.314$ *and* 0.6 μm. '×' denotes the maximum point.

Fig. 6 presents the variation of two dimensionless parameters derived from the proposed model, i.e., $H^* = \Delta H_g(2H - \Delta H_g)/\mu^2$ and $A^* = a/a^*$, with respect to the sample depth h for a SNC IF steel sample at $\varepsilon_e = 0.25$ in the GSG region. In view of the fact that the measured ΔH_g was available in the range of $h \in (0, 120\ \mu m)$, i.e., within the thickness of the GSG region, and u was not available in the range of $h \in (0, 50\ \mu m)$, only the results of A^* in the range of $h \in (50, 120\ \mu m)$ are presented. The results show that the values of both parameters first increase to a maximum value and then decrease, and they are comparable in magnitude. The influence of Δh is also studied by varying its value, i.e., $\Delta h =$ 0.2, 0.314 *and* 0.6 μm. The smaller the value of Δh, the larger the parameter A^*. The value of A^* at $\Delta h = 0.314\ \mu m$ is in good agreement with that of H^* at large h, i.e., $h \in (80, 120\ \mu m)$, and they approximately approach an equal maximum value at the same sample depth h, i.e., the value of H^* reaches a maximum (i.e., $H^*_{max} = 22.64 \times 10^{-5}$) at $h = 82.3\ \mu m$, while that of A^* reaches a maximum (i.e., $A^*_{max} = 22.62 \times 10^{-5}$) at $h = 89\ \mu m$, see the crosses in the figure.

The significant quantitative difference between the two parameters at small h might be due to several reasons as explained below. Firstly, there was a significant influence of noise on the height profile data, as indicated by the symbols in Fig. 5 in the range of around $h \in (0, 80\ \mu m)$, due to the lateral surface roughness [30]. Secondly, the outermost surface (i.e., xz plane at $h = 0$ in Fig. 2) could affect the measurement of the height profile near the said surface due to the surface effect. Thirdly, it can be seen from Fig. 5 that the eight height profiles differ from each other, which indicates that the height profile was not uniform along the tensile

direction (i.e., z axis in Fig. 2) while in our model the height profile is assumed to be uniform and the GNDs are also assumed to be uniformly distributed in a localized region near the lateral surface. The non-uniformity of the measured height profile could be caused by the non-uniform peening of steel balls on the outermost surface in the SMAT process. Furthermore, the extra hardening ΔH_g was expressed as $(\Delta H_{SNC} - \Delta H_{free\ GSG})$ in which the ΔH values of various free standing layers with different grain sizes have been approximated as those of the layers in a free standing GSG sample, i.e., $\Delta H_{free\ GSG}$, due to the impossibility of measuring the ΔH value of the free standing layers. Finally, the effect of the compressive residual stresses in the surface layer generated in the process of SMAT [40] on the hardness of SNC materials was ignored in our model. Actually, existing investigations have shown that compressive residual stresses would enhance hardness, whereas tensile residual stresses would decrease hardness [41,42]. Therefore, the maximum compressive residual stresses of around 500 MPa in a SNC steel sample [40] could produce a maximum hardness enhancement of around 10% in the top surface layer.

The first three reasons could produce errors in measuring height profiles (i.e., the value of A^*) while the last two could produce calculation errors for H^*. It is important to note that a small error in u, especially the noise (zigzag in Fig. 5), could generate a significant error in calculating its slope, i.e., the value of parameter a (a should be larger than zero, see Fig. 4b), due to the limited experimental data for smoothening at small h, i.e., $h \in (50, 60\ \mu m)$. Consequently, the slopes of the eight height profiles near the surface, which are critical in determining the value of A^*, are not accurate and in some cases negative slopes occur at small h in some height profiles even though the measured data have been carefully smoothened using the fnval Matlab function (see the short dashed lines in Fig. 5). This explains the presence of the negative values of A^* in the approximate range of $h \in (50, 60\ \mu m)$, and the obvious quantitative difference between H^* and A^* at small h, i.e., $h \in (50, 80\ \mu m)$, as shown in Fig. 6.

In view of the above reasons, the two parameters are deemed in agreement with each other at least qualitatively. This agreement validates the proposed law on correlation of the extra strain hardening achieved in the GSG structure with the non-uniform deformation resulting from the GSG structure. In other words, the extra strain hardening ΔH_g can be quantitatively determined by the height profile u, which could be measured from experiments. The proposed law has also demonstrated the success of adopting the concept of GNDs in describing the remarkable extra hardening in the GSG layer due to the presence of the gradient structure. Indeed, Wu et al. [30] observed a dislocation density up-turn at strain $\varepsilon_e \in (0.015, 0.05)$ in a stress relaxation experiment for a SNC IF steel sample, as shown in their Fig. 4(b). A combination of the above observations and our model predictions has demonstrated that the injections of GNDs into the SNC IF steel sample, which are induced by the non-homogeneous deformation in the lateral surface, are due to the existence of the special gradient structure.

The dimensionless parameter H^* of SNC samples for other strain values (i.e., $\varepsilon_e = 0.05,\ 0.10$) is presented in Fig. 7, which shows that the trend of H^* versus h is similar to that of $\varepsilon_e = 0.25$ but the former H^* has smaller values. In general, the higher the strain, the larger the value of H^* is. The value of A^* is unavailable due to the difficulty of measuring the lateral surface topography accurately at smaller tensile strains. Nevertheless, based on the above results it is reasonable to infer that the variation of height profile u at a smaller strain is similar to that at $\varepsilon_e = 0.25$ but with a smaller slope, which leads to a smaller a and A^*. Moreover, it is interesting to note from Fig. 7 that the H^* maximums for all the applied strains are reached at approximately the same sample depth, i.e., $h \approx 80\ \mu m$, which reveals the depth where the maximum strain gradient occurs in the SNC sample. In other words, unlike ΔH or ΔH_g, the position of the H^* peak is independent of the applied strain; and it only depends on the specific GSG structure.

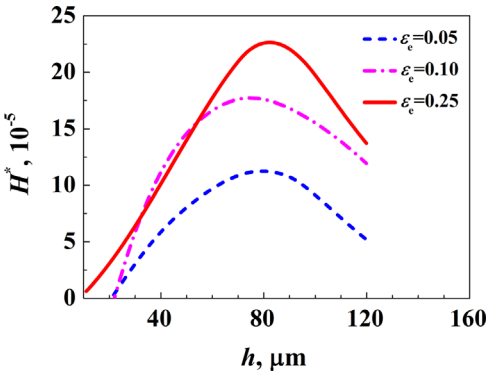

Fig. 7. Variation of dimensionless parameter $H^* = \Delta H_g(2H - \Delta H_g)/\mu^2$ of a SNC IF steel sample with respect to the sample depth h at various tensile strains (i.e., $\varepsilon_e = 0.05$, 0.1 and 0.25).

5. Concluding remarks

Based on the concept proposed by Gao et al. [43] that GNDs were generally correlated with strain gradient, we found that the density of GNDs (Eq. (5)) induced by the GSG structure can be recast as a function of strain gradient, i.e., $\rho_{GSG} = a/[b(\Delta h)^2] = \eta_{GSG}/b$, where $\eta_{GSG} = a/(\Delta h)^2$ is the strain gradient in a unit layer and its value depends on the height profile and thus varies from the topmost surface to the interior. The mentioned value is also dependent on the magnitude of the tensile strain, as shown in Fig. 7. Moreover, the maximums in Figs. 6 and 7 indicate where the maximum strain gradient occurs in a SNC sample. By modifying our previous plasticity model for SNC materials [29], it is likely that a continuum plasticity model for SNC materials can be developed to quantitatively describe the GSG-dependent extra hardening and ductility in SNC materials, which would be beneficial in optimizing their strength and ductility balance.

Although the quantitative correlation between the extra hardening and the non-uniform deformation in the lateral surface of a SNC sample has been clearly identified by the proposed physical law in a simple form, the developed model has some limitations due to the assumptions and approximations adopted. For example, the predictions of the proposed model would be inaccurate when the material in the same layer is heterogeneous or when the non-uniform deformation in the lateral surface along the tensile direction is not uniform. Moreover, we were compelled to adopt an approximated expression for the extra hardening ΔH_g due to the difficulty encountered in measuring the hardness increments ΔH of free standing layers with different grain sizes. The proposed model is thus prone to some errors in quantitatively correlating ΔH_g and the non-uniform deformation in the lateral surface of a SNC sample. Therefore, some other models should be established to circumvent the above limitations. For example, by combining the continuum plasticity model for SNC materials developed by some of the authors [29], a three-dimensional shear-lag model [35,36] or a crystal plasticity model [44] with the activity of GNDs incorporated [45] could be a feasible choice for quantitatively predicting the lateral non-uniform deformation, the hardness increments of the free standing layers with different grain sizes and, hence the macro mechanical behavior of the SNC samples. The GSG structure could then be tailored to tune the lateral non-uniform deformation such that the extra hardening grains in the SNC sample is optimized, which could in return enhance the synergy of high strength and high ductility in the SNC samples.

In summary, we have developed a physical model to correlate the strong extra strain hardening achieved in a grain size gradient structure with the non-uniform deformation in the lateral surface of a SNC material based on the existing experimental observations and the concept of GNDs. The above model resulted in a physical law in the simple form of $H^* = A^*$, where $H^* = \Delta H_g(2H - \Delta H_g)/\mu^2$ and $A^* = a/a^*$ are two dimensionless parameters that can be measured from experiments. The former parameter represents the extra strain hardening and the latter characterizes the non-uniform deformation in the lateral surface embodied by its height profile.

Acknowledgments

This work was supported by the National Natural Science Foundation of China (NSFC) (11402203), the Fundamental Research Funds for the Central Universities (3102014JCQ01039) and the Start-up Funds for the Newly-recruited High-level Talents from Northwestern Polytechnical University, China. S.C. thanks the support from NSFC through Grants #11125211, #11372317 and the 973 Nano-project (2012CB937500). A.K. Soh acknowledges the support of the Advanced Engineering Programme and School of Engineering, Monash University Malaysia, as well as the eScience Grant (Project no.: 06-02-10-SF0195) provided by the Ministry of Science, Technology and Innovation (MOSTI), Malaysia.

References

[1] M.A. Meyers, A. Mishra, D.J. Benson, Prog. Mater. Sci. 51 (2006) 427–556.
[2] M. Dao, L. Lu, R. Asaro, J. De Hosson, E. Ma, Acta Mater. 55 (2007) 4041–4066.
[3] H. Gleiter, Prog. Mater. Sci. 33 (1989) 223–315.
[4] D.S. Gianola, S. Van Petegem, M. Legros, S. Brandstetter, H. Van Swygenhoven, K.J. Hemker, Acta Mater. 54 (2006) 2253–2263.
[5] J. Li, A.K. Soh, X. Wu, Scr. Mater. 78–79 (2014) 5–8.
[6] J. Li, A.K. Soh, Appl. Phys. Lett. 101 (2012) 241915.
[7] J. Li, A.K. Soh, Acta Mater. 61 (2013) 5449–5457.
[8] J. Li, S. Chen, Mater. Lett. 121 (2014) 174–176.
[9] X. Wu, Y. Zhu, Y. Wei, Q. Wei, Phys. Rev. Lett. 103 (2009) 205504.
[10] K. Lu, L. Lu, S. Suresh, Science 324 (2009) 349–352.
[11] J. Li, A.K. Soh, Philos. Mag. Lett. 92 (2012) 690–700.
[12] Y.M. Wang, M.W. Chen, F.H. Zhou, E. Ma, Nature 419 (2002) 912–915.
[13] K. Lu, J. Lu, J. Mater. Sci. Technol. 15 (1999) 193–197.
[14] T.H. Fang, W.L. Li, N.R. Tao, K. Lu, Science 331 (2011) 1587–1590.
[15] M. Guagliano, J. Mater. Process. Technol. 110 (2001) 277–286.
[16] M. Umemoto, Y. Todaka, K. Tsuchiya, Mater. Trans. 44 (2003) 1488–1493.
[17] C.L. Rountree, R.K. Kalia, E. Lidorikis, A. Nakano, L. Van Brutzel, P. Vashishta, Annu. Rev. Mater. Sci. 32 (2002) 377–400.
[18] Z. Pu, S. Yang, G.L. Song, O. Dillon Jr, D. Puleo, I. Jawahir, Scr. Mater. 65 (2011) 520–523.
[19] Y. Todaka, M. Umemoto, Y. Watanabe, K. Tsuchiya, Designing, Processing and Properties of Advanced Engineering Materials, Pts 1 and 2, in: S.G. Kang, T. Kobayashi (Eds.), Trans Tech Publications Ltd, Zurich-Uetikon, 2004, pp. 1149–1152.
[20] J.W. Tian, K. Dai, J.C. Villegas, L. Shaw, P.K. Liaw, D.L. Klarstrom, A.L. Ortiz, Mater. Sci. Eng. A 493 (2007) 176–183.
[21] X. Wu, N. Tao, Y. Hong, B. Xu, J. Lu, K. Lu, Acta Mater. 50 (2002) 2075–2084.
[22] X. Lu, Q. Lu, Y. Li, L. Lu, Sci. Rep. 3 (2013) 3319.
[23] K. Wang, N.R. Tao, G. Liu, J. Lu, K. Lu, Acta Mater. 54 (2006) 5281–5291.
[24] J.W. Tian, L. Shaw, P.K. Liaw, K. Dai, Mater. Sci. Eng. A 498 (2008) 216–224.
[25] J. Li, S. Chen, X. Wu, A.K. Soh, J. Lu, Mater. Sci. Eng. A 527 (2010) 7040–7044.
[26] A.Y. Chen, H.H. Ruan, J. Wang, H.L. Chan, Q. Wang, Q. Li, J. Lu, Acta Mater. 59 (2011) 3697–3709.
[27] J. Li, A.K. Soh, Modell. Simul. Mater. Sci. Eng. 20 (2012) 085002.
[28] H.H. Ruan, A.Y. Chen, J. Lu, Mech. Mater. 42 (2010) 559–569.
[29] J. Li, A.K. Soh, Int. J. Plast. 39 (2012) 88–102.
[30] X. Wu, P. Jiang, L. Chen, F. Yuan, Y.T. Zhu, Proc. Natl. Acad. Sci. USA 111 (2014) 7197–7201.
[31] H. Gao, Y. Huang, Scr. Mater. 48 (2003) 113–118.
[32] W.D. Nix, H.J. Gao, J. Mech. Phys. Solids 46 (1998) 411–425.
[33] M. Ashby, Philos. Mag. 21 (1970) 399–424.
[34] M.E. Gurtin, Int. J. Plast. 24 (2008) 702–725.
[35] G. Jiang, K. Peters, Int. J. Solids Struct. 45 (2008) 4049–4067.
[36] J.A. Nairn, D.-A. Mendels, Mech. Mater. 33 (2001) 335–362.
[37] L.L. Zhu, H.H. Ruan, X.Y. Li, M. Dao, H.J. Gao, J. Lu, Acta Mater. 59 (2011) 5544–5557.
[38] L.L. Zhu, J. Lu, Int. J. Plast. (2012) 166–18430–31 (2012) 166–184.
[39] W.L. Li, N.R. Tao, K. Lu, Scr. Mater. 59 (2008) 546–549.
[40] J. Lu, K. Lu, Surface nanocrystallization (SNC) of materials and its effect on mechanical behavior, in: I. Milne, R.O. Ritchie, B. Karihaloo (Eds.), Comprehensive Structural Integrity, Elsevier, Oxford, 2003, pp. 495–528.
[41] G. Pharr, T. Tsui, A. Bolshakov, W. Oliver, MRS Proceedings, Cambridge University Press (1994) 127.
[42] N. Huber, J. Heerens, Acta Mater. 56 (2008) 6205–6213.
[43] H. Gao, Y. Huang, W.D. Nix, J.W. Hutchinson, J. Mech. Phys. Solids 47 (1999) 1239–1263.
[44] P.D. Wu, D.J. Lloyd, M. Jain, K.W. Neale, Y. Huang, Int. J. Plast. 23 (2007) 1084–1104.
[45] A. Ma, F. Roters, D. Raabe, Acta Mater. 54 (2006) 2169–2179.